# Abundance Patterns of $\alpha$ and Neutron-capture Elements in the Helmi Stream

Guilherme Limberg[1] , Rafael M. Santucci[2,3] , Silvia Rossi[1] , Anna B. A. Queiroz[4,5] , Cristina Chiappini[4,5] ,
Stefano O. Souza[1] , Hélio D. Perottoni[1] , Angeles Pérez-Villegas[6] , and Fabrícia O. Barbosa[1]

[1] Universidade de São Paulo, Instituto de Astronomia, Geofísica e Ciências Atmosféricas, Departamento de Astronomia, SP 05508-090, São Paulo, Brazil
guilherme.limberg@usp.br
[2] Universidade Federal de Goiás, Instituto de Estudos Socioambientais, Planetário, Goiânia, GO 74055-140, Brazil
[3] Universidade Federal de Goiás, Campus Samambaia, Instituto de Física, Goiânia, GO 74001-970, Brazil
[4] Leibniz-Institut für Astrophysik Potsdam (AIP), An der Sternwarte 16, D-14482 Potsdam, Germany
[5] Laboratório Interinstitucional de e-Astronomia—LIneA, RJ 20921-400, Rio de Janeiro, Brazil
[6] Instituto de Astronomía, Universidad Nacional Autónoma de México, Apartado Postal 106, C.P. 22800, Ensenada, B.C., México
Received 2021 March 30; revised 2021 May 11; accepted 2021 May 12; published 2021 June 1

## Abstract

We identified eight additional stars as members of the Helmi stream (HStr) in the combined GALAH+ DR3 and Gaia EDR3 catalog. By consistently reevaluating claimed members from the literature, we consolidate a sample of 22 HStr stars with parameters determined from high-resolution spectroscopy and spanning a considerably wider (by $\sim$0.5 dex) metallicity interval ($-2.5 \lesssim$ [Fe/H] $< -1.0$) than previously reported. Our study focuses on $\alpha$ (Mg and Ca) and neutron-capture (Ba and Eu) elements. We find that the chemistry of HStr is typical of dwarf spheroidal (dSph) galaxies, in good agreement with previous $N$-body simulations of this merging event. Stars of HStr constitute a clear declining sequence in [$\alpha$/Fe] for increasing metallicity up to [Fe/H] $\sim -1.0$. Moreover, stars of HStr show a median value of $+0.5$ dex for [Eu/Fe] with a small dispersion ($\pm 0.1$ dex). Every star analyzed with [Fe/H] $< -1.2$ belongs to the $r$-process enhanced ([Eu/Fe] $> +0.3$ and [Ba/Eu] $< 0.0$) metal-poor category, providing remarkable evidence that, at such a low-metallicity regime, stars of HStr experienced enrichment in neutron-capture elements predominantly via $r$-process nucleosynthesis. Finally, the extended metallicity range also suggests an increase in [Ba/Eu] for higher [Fe/H], in conformity with other surviving dwarf satellite galaxies of the Milky Way.

*Unified Astronomy Thesaurus concepts:* Dwarf galaxies (416); Milky Way stellar halo (1060); Milky Way dynamics (1051); Milky Way evolution (1052); Milky Way formation (1053); Population II stars (1284); Stellar populations (1622); Chemical abundances (224); R-process (1324)

## 1. Introduction

Within the hierarchical assembly paradigm, the Galactic stellar halo (or simply "halo") is expected to retain the chemodynamical signatures of merging events between the Milky Way and dwarf galaxies of various masses in the past (Helmi 2008, 2020). Therefore, studies of surviving satellite galaxies provide insights about the formation of the Milky Way itself. Unfortunately, measurements of elemental abundances in the atmospheres of individual stars from these distant systems are extremely difficult (e.g., Tolstoy et al. 2009), hindering our ability to directly investigate their star-forming environments and chemical-evolution histories.

An alternative approach is to pinpoint which stars in the halo were accreted and, out of these, which ones share a common origin. A widely utilized strategy to find the stellar remnants of these ancient building blocks is to search for their clumping in phase space. The first identification of a kinematically cohesive group of stars with this method was presented in a seminal work by Helmi et al. (1999). Throughout the years, this substructure has been known as the Helmi stream (hereafter HStr; see Helmi 2020 for a recent review).

In order to investigate the chemical profile of HStr, Roederer et al. (2010) observed 12 likely members of this substructure. More recently, Aguado et al. (2021b) acquired spectra for seven more candidates. Interestingly, both efforts reported that stars of HStr were enriched in neutron-capture elements predominantly via the rapid process ($r$-process) in comparison to the slow one ($s$-process; see Sneden et al. 2008 and

Frebel 2018 for reviews). In recent studies, Limberg et al. (2021a) and Gudin et al. (2021) demonstrated that, indeed, several $r$-process-enhanced (RPE; [Eu/Fe] $> +0.3$ and [Ba/Eu] $< 0.0$) metal-poor ([Fe/H] $< -1.0$; Beers & Christlieb 2005) stars are dynamically associated with HStr. It appears that chemical-abundance information for larger samples of genuine members of HStr might allow us to investigate the site (s) for the occurrence of the $r$-process in its (now) destroyed progenitor system. In addition, stars of HStr have the enormous advantage of being much closer (and hence brighter) than any surviving dwarf spheroidal (dSph) or ultra-faint dwarf (UFD) satellite galaxy.

In this Letter, we identified additional stars of HStr in the third data release (DR3) of the Galactic Archaeology with HERMES (GALAH+ DR3; Buder et al. 2021) survey combined with Gaia Early Data Release 3 (EDR3; Gaia Collaboration et al. 2021). We also searched the literature to consolidate a sample covering an [Fe/H] interval considerably wider than previously reported. The extended metallicity range reveals a declining trend in [$\alpha$/Fe] within $-2.0 \lesssim$ [Fe/H] $< -1.0$, providing clear evidence that HStr is the debris of a long-vanished dwarf galaxy. This sample further allowed us to investigate neutron-capture elements. We demonstrate that the [Ba/Eu] pattern is consistent with the dwarf-galaxy progenitor hypothesis. We also confirm that every star of HStr with [Fe/H] $< -1.2$ belongs to the aforementioned RPE class. The employed data is described in Section 2. Section 3 contains our dynamical and chemical analyses. The summary of our results and a brief discussion are presented in Section 4.
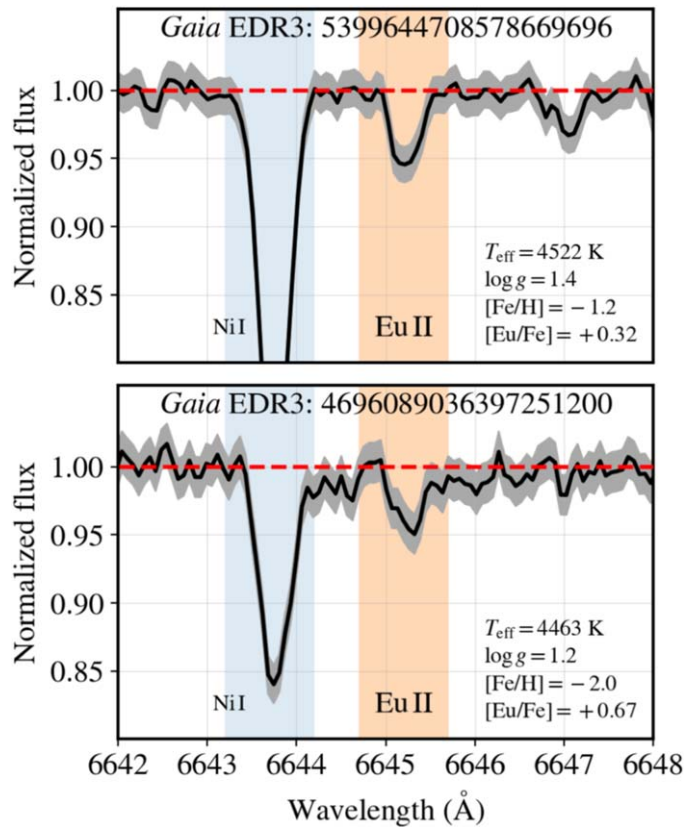
**Figure 1.** Examples of GALAH+ DR3 spectra in the wavelength region of the Eu II line (6645 Å; orange-shaded area). For the convenience of the reader, we also identify the strong absorption feature as Ni I (blue stripe). Both panels show stars selected as confident members of HStr (see Section 3.1). The black solid lines are the normalized spectra, while the gray-shaded regions represent their respective $1\sigma$ uncertainties. The red dashed line shows the position of the pseudocontinuum to guide the eye.

## 2. Data

### 2.1. Stream Candidates

We considered the complete GALAH+ DR3 high-resolution ($R \sim 28,000$) spectroscopic catalog. First, we removed stars with flagged[7] stellar parameters (flag_sp $\neq 0$) and metallicities (flag_fe_h $\neq 0$). Since we are interested in finding stars associated with a substructure of low metallicity, we further constrain our sample to [Fe/H] $\leqslant -0.7$ (keeping $\sim$18,000 stars). Moreover, all abundances analyzed (Sections 3.2 and 3.3) are true measurements (flag_X_fe $= 0$, where X is any given chemical species). We put particular attention to the estimated [Eu/Fe], since it relies on a single line in GALAH, Eu II at 6645 Å, which is difficult to detect in warm metal-poor stars (Sneden et al. 2008). Hence, all stars with reliable [Eu/Fe] in the sample are in the upper-giant-branch phase ($T_{\rm eff} < 4800$ K and $\log g < 2.0$). At this wavelength, the typical signal-to-noise ratio is $60 \leqslant$ snr_c3_iraf $\leqslant 80$ for these objects. We also visually inspected the spectra of stars found to be associated with HStr (Section 3.1) to ensure the presence of this absorption feature (see Figure 1).

To achieve a more complete view of the chemical patterns of HStr, over a large metallicity range, we also compiled stars that had been previously suggested to be associated with the substructure. We require that these stars have atmospheric parameters and abundances estimated from analyses of high-

resolution spectra, in conformity with GALAH. The fundamental source is Aguado et al. (2021b), because these authors had already performed a search in the literature for HStr candidates. This sample includes stars observed mostly by the authors themselves and by Roederer et al. (2010). It also contains stars, attributed to HStr by Yuan et al. (2020), observed over the course of the Apache Point Observatory Galactic Evolution Experiment (APOGEE; Majewski et al. 2017) survey. We have further included stars indicated by Limberg et al. (2021a) and Gudin et al. (2021) in our literature compilation. Stellar parameters and abundances for these references were obtained during the main effort of the $R$-Process Alliance (Hansen et al. 2018; Ezzeddine et al. 2020).

### 2.2. Dynamical Properties

We cross-matched (1″5 search radius) all samples with Gaia EDR3 to acquire accurate parallaxes (recalibrated following Lindegren et al. 2021a) and absolute proper motions. These astrometric information, the high-resolution spectroscopic data (Section 2.1), as well as mid- and near-infrared photometry from the Wide-field Infrared Survey Explorer (WISE; Wright et al. 2010) and the Two Micron All Sky Survey (2MASS; Skrutskie et al. 2006), respectively, were used to estimate heliocentric distances via isochrone fitting in a Bayesian framework with the StarHorse code (Queiroz et al. 2018). For this exercise, we did not consider targets classified as spurious astrometric solutions (fidelity_v1 $< 0.5$; Rybizki et al. 2021). The medians of the resulting posterior probability distribution functions were taken as nominal values (see the

---

[7] Whenever a quality flag is set to zero in the GALAH+ DR3 catalog, it represents a reliable and/or real estimate of the given parameter. For details on the quality assessment, we refer the reader to Buder et al. (2021).
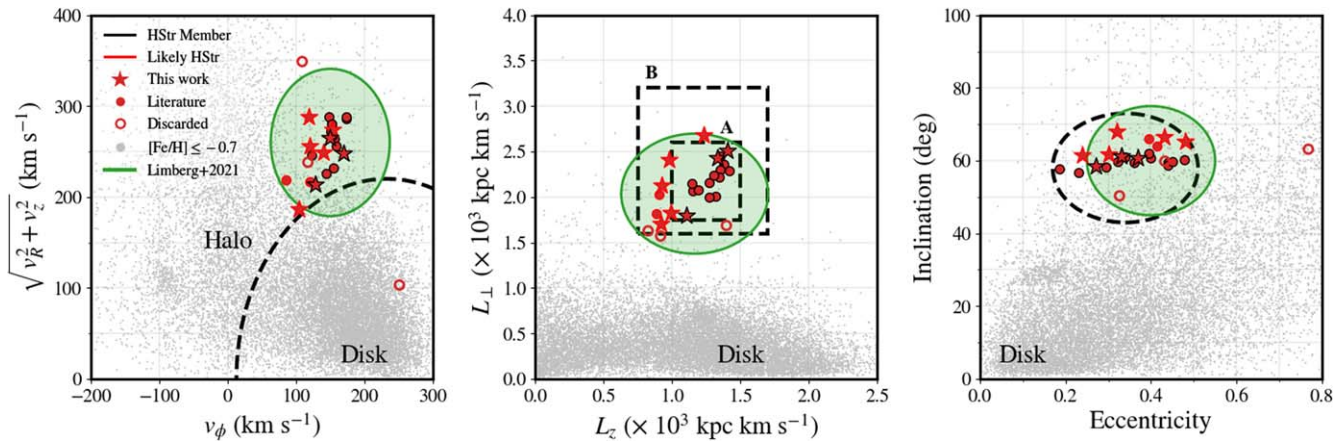
**Figure 2.** Left: velocity distribution. The dashed line marks the $||\mathbf{v} - \mathbf{v}_{\rm circ}|| \geqslant 220$ km s$^{-1}$ boundary between the disk and the halo (see the text). Middle: $(L_z, L_\perp)$. The dashed lines delineate the selection boxes (A and B; see Section 3.1) from Koppelman et al. (2019). Right: inclination vs. eccentricity. The dashed ellipse marks the selection from Aguado et al. (2021b). Green ellipses delimit $3\sigma$ ranges for the distributions of HStr stars presented by Limberg et al. (2021a). In all of the panels, the regions dominated by disk-like orbits are also indicated. Stream members are shown as red symbols with black (confident) or red (likely) edges. Open symbols are discarded candidates. Star symbols are members selected from the GALAH sample and circles are from the literature compilation. Gray dots represent low-metallicity ([Fe/H] $\leqslant -0.7$) stars from GALAH.

Appendix). We refer to Queiroz et al. (2020) for a complete description of the assumptions regarding the stellar-evolution models and priors. We also discarded stars with renormalized unit weight errors of the reduced astrometric $\chi^2$ outside the recommended interval (RUWE > 1.4; Lindegren et al. 2021b) and those with relative uncertainties $\geqslant 15\%$ in their derived distances.

Given the high quality of the spectra at hand, we considered radial velocities (RVs) from the various sources mentioned in Section 2.1. For the targets observed by Aguado et al. (2021b), neither improved RVs were determined by the authors nor these are provided by Gaia's data releases. Hence, we adopted RVs from the low-resolution spectroscopy of Sloan Digital Sky Survey (SDSS)/SEGUE (York et al. 2000; Yanny et al. 2009) and Large Sky Area Multi-Object Fiber Spectroscopic Telescope (LAMOST; Cui et al. 2012), with errors no worse than 5 km s$^{-1}$.

We calculated the orbits of all stars for 5 Gyr forward, with the publicly available library AGAMA (Vasiliev 2019), under the axisymmetric Galactic potential model of McMillan (2017). The Galactic parameters are, for consistency, from McMillan (2017) as well. Specifically, the distance from the Sun to the Galactic center is $R_\odot = 8.2$ kpc, the circular velocity at this position is $v_{\rm circ} = 232.8$ km s$^{-1}$, and the peculiar motion of the Sun is $(U, V, W)_\odot = (11.10, 12.24, 7.25)$ km s$^{-1}$ (Schönrich et al. 2010). We accounted for the uncertainties in distances, proper motions, and RVs, assuming Gaussian profiles for those, by performing 1000 realizations of each star's orbit with a Monte Carlo procedure. The medians of the resulting distributions were taken as our characteristical values in the derived dynamical quantities.

## 3. Analysis

### 3.1. Stream Membership

In order to accomplish a consistent analysis of abundance information (Sections 3.2 and 3.3), it is necessary to delineate a clear stream membership criteria. Then, we need to implement such selection consistently for all samples described in Section 2. Conveniently, previous studies carried out similar exercises for HStr.

First, we removed stars with disk-like kinematics utilizing the plane defined by $(v_\phi, \sqrt{v_R^2 + v_z^2})$, where $(v_R, v_\phi, v_z)$ is the velocity vector in the cylindrical coordinate system. Stars with $v_\phi > 0$ are in prograde motion, rotating in the same orientation as the disk. For this purpose, we applied the cut $||\mathbf{v} - \mathbf{v}_{\rm circ}|| \geqslant 220$ km s$^{-1}$ (dashed line in the left panel of Figure 2), where $\mathbf{v}$ is the complete velocity vector of a given star.

Second, we employed the criteria suggested by Koppelman et al. (2019), who carried out an in-depth chemodynamical characterization of HStr. These authors' selection boxes are drawn in the middle panel of Figure 2 within the space defined by the in-plane ($L_\perp$) and vertical ($L_z$) components of the total angular momentum ($L = \sqrt{L_\perp^2 + L_z^2}$). For prograde motion, $L_z > 0$. Although $L_\perp$ is not fully conserved in an axisymmetric potential, it is commonly used for the identification of substructures since it preserves a reasonable amount of clumping over time (e.g., Helmi 2008, 2020). Stars that respect the more restrictive box (A) are considered confident members of the stream (symbols with black edges), while objects occupying the more permissive one (B) are taken to be likely associated (red edges).

The third criterion used in this work is equivalent to the one described by Aguado et al. (2021b), characterized by orbital inclination ($i = \arccos(L_z/L)$; from this definition, $i < 90°$ for prograde motion) and eccentricity. These authors vetted their stream candidates with a $4\sigma$ range around the center of the distribution of HStr members originally found by Myeong et al. (2018) in this parameter space. In the right panel of Figure 2, the dashed ellipse reproduces these authors' selection.

A comparison between these criteria and the $3\sigma$ distributions of HStr stars from Limberg et al. (2021a) is also provided in all of the panels of Figure 2 (green ellipses). The application of this three-step selection to the low-metallicity sample from GALAH yields a total of eight HStr candidates (red star symbols). Out of these, three stars are classified as confident and five are classified as probable members. We also evaluated the literature compilation with the same approach, resulting in a total of 14 additional stars to be considered for the analysis of chemical-abundance data (red circles). Among these stars, four are originally from Roederer et al. (2010), three are from
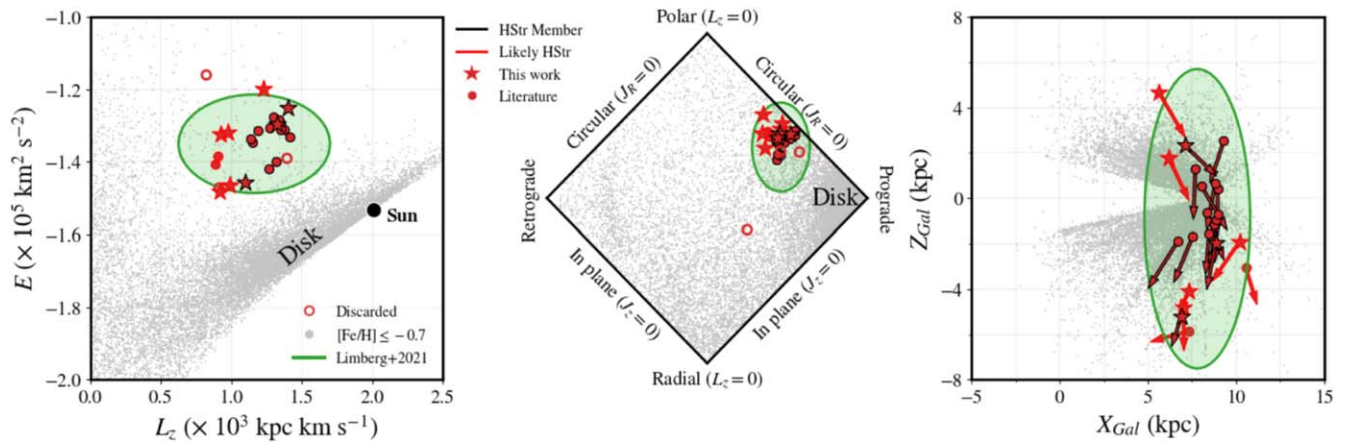
**Figure 3.** Left: ($L_z$, $E$). Middle: action-space map. In both panels, the regions dominated by disk-like orbits are also indicated. Right: HStr stars in Cartesian Galactic positions ($X$, $Z$)$_{Gal}$. The arrows point in the directions of the motion of the stars, scaled by their amplitudes. Green ellipses delimit $3\sigma$ ranges for the distributions of the HStr stars presented by Limberg et al. (2021a). In all panels, stream members are shown as red symbols with black (confident) or red (likely) edges. Open symbols are discarded candidates. Star symbols are members selected from the GALAH sample and circles are from the literature compilation (Section 2.1). Gray dots represent low-metallicity ([Fe/H] $\leqslant -0.7$) stars from GALAH.

Yuan et al. (2020), and five were observed by Aguado et al. (2021b). The single star selected from Limberg et al. (2021a) has been confirmed to be associated with the stream, while only one from Gudin et al. (2021) can be considered a member. The final list of 22 vetted HStr stars, alongside relevant information about them, is provided in the Appendix.

As a sanity check, we have examined the newly identified stream members in orbital energy ($E$) and actions ($J_R$, $J_\phi = L_z$, and $J_z$). For consistency, these are also compared to the distributions independently found by Limberg et al. (2021a). In Figure 3, we show the $3\sigma$ ranges for HStr found by these authors in ($L_z$, $E$) and in the action-space map (left and middle panels, respectively). All confident members overlap with the delineated regions, while a couple of the probable ones fall outside of them, but are located near the boundaries. This qualitative inspection helps consolidate our set of criteria as truly representative of HStr.

Despite carrying out a selection exclusively with a kinematic/dynamical approach, stars of HStr are cohesively distributed in configuration space (right panel of Figure 3). These objects are piercing through the Galactic plane, streaming downwards in the Cartesian Galactic position plane ($X$, $Z$)$_{Gal}$. Such behavior is commonly interpreted as the partial phase mixing of the debris of a shredded dwarf galaxy (Helmi 2008; Myeong et al. 2018; Koppelman et al. 2019).

### 3.2. α Elements

With our collection of 22 stream members (15 confident and 7 likely), we investigate abundance trends of $\alpha$ elements (Mg and Ca) derived exclusively from high-resolution spectroscopy. In this context, we can compare our [$\alpha$/Fe]–[Fe/H] distributions with those presented by Aguado et al. (2021b), who analyzed a mixture between low- and high-resolution data. We can also compare these chemical-abundance patterns with those from surviving dwarf satellite galaxies of the Milky Way and speculate about the nature of HStr's parent system.

We present the $\alpha$-element profiles in the top row of Figure 4. The most prominent, immediately perceptible feature is the clear decrease in [$\alpha$/Fe] (both Mg and Ca) with increasing metallicity, but plateauing at $\sim 0.35$ for [Fe/H] $\lesssim -2.0$, characterizing a "knee" (e.g., Matteucci & Greggio 1986).

This point delimits the transition between core-collapse and SNe Ia dominated epochs in chemical evolution and was first conjectured for external galaxies by Matteucci & Brocato (1990), later observed by Shetrone et al. (2003). A similar $\alpha$-pattern signature was presented by Aguado et al. (2021b). However, their results were limited to lower metallicities ([Fe/H] $\lesssim -1.5$). Hence, the inclusion of the GALAH sample confirms the continuity of this $\alpha$-element trend of HStr stars up to [Fe/H] $\sim -1.0$ with an excellent agreement. We stress that considering exclusively the newly found members from GALAH, this pattern is still noticeable. Consequently, even if small biases between sources might exist, these qualitative conclusions are robust against them.

The comparison to dwarf satellite galaxies of the Milky Way is presented in Figure 4 as well. Abundances have been compiled from the Stellar Abundances for Galactic Archaeology (SAGA) database (Suda et al. 2008, 2017), favoring references with neutron-capture elements available. The Sculptor dSph (Hill et al. 2019) follows a similar sequence in [$\alpha$/Fe] for the same metallicity range ($-2.5 \lesssim$ [Fe/H] $\lesssim -1.0$) to that of HStr stars, but with a steeper decline. With the aid of chemical-evolution models, such a feature has been interpreted by Aguado et al. (2021b) as a dSph-galaxy progenitor with a slower star formation rate, but accompanied by a smaller wind efficiency, when compared to Sculptor. This apparent dSph-like origin is in keeping with previous $N$-body simulations of this merging event by Koppelman et al. (2019).

### 3.3. Neutron-capture Elements

In this work, we are also interested in evaluating the hypothesis that the progenitor of HStr was enriched in neutron-capture elements (Ba and Eu) predominantly via the $r$-process, as suggested by Roederer et al. (2010; and followed-up by Aguado et al. 2021b) and reinforced with a dynamical counterpart to the argument by Limberg et al. (2021a; also Gudin et al. 2021). Here, we consider the abundances of Ba and Eu, since these chemical species serve as diagnostics for the $r$-process enhancement in metal-poor stars as first noted by Spite (1992), although the existence of this kind of object was established much earlier by Spite & Spite (1978). Roederer et al. (2010) were capable of determining abundances of these
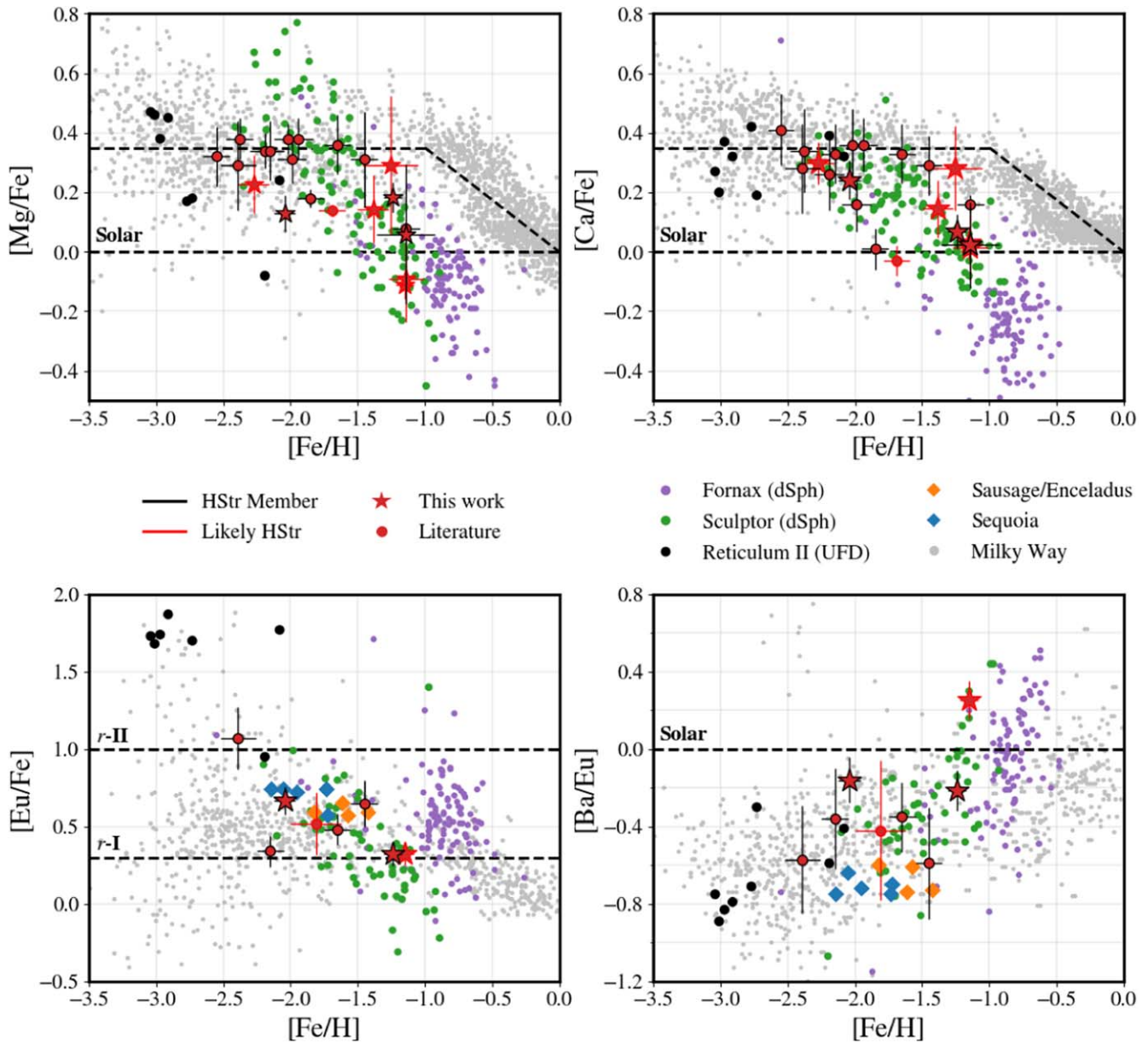
**Figure 4.** Top row: α elements, [Mg/Fe] (left) and [Ca/Fe] (right) vs. [Fe/H]. Upper dashed lines approximately follow the evolution of the Milky Way, with a knee at [Fe/H] = −1.0 (e.g., Matteucci & Greggio 1986). The solar level is also indicated in both panels. Bottom row: neutron-capture elements. Left: [Eu/Fe]–[Fe/H]. The dashed lines at [Eu/Fe] = +0.3 and +1.0 delineate the characteristic r-process enhancement of the r-I and r-II, respectively, classes of RPE metal-poor stars (Beers & Christlieb 2005). Right: [Ba/Eu]–[Fe/H]. The solar level is marked as well. In all of the panels, stream members are shown as red symbols with black (confident) or red (likely) edges. Star symbols are members selected from the GALAH sample and circles are from the literature compilation (Section 2.1). Colored dots illustrate stars from dSph or UFD galaxies compiled in the SAGA database (Suda et al. 2008, 2017). Purple: Fornax (dSph; Letarte et al. 2010; Lemasle et al. 2014). Green: Sculptor (dSph; Hill et al. 2019). Black: Reticulum II (UFD; Ji et al. 2016). Dark-blue and dark-red diamonds are stars from Gaia-Sausage/Enceladus and Sequoia, respectively, observed by Aguado et al. (2021a). Gray dots in all panels are Milky Way stars, also from the SAGA database. We complement these with data from the r-process alliance (Gudin et al. 2021).

elements for some of their stream candidates. Out of four stars observed by these authors and vetted as confident members (Section 3.1), three of them have [Ba/Fe] and [Eu/Fe] measured. All stream stars from the GALAH sample have nonflagged (flag_Ba_fe = 0) [Ba/Fe], but only three of them have usable (flag_Eu_fe = 0) Eu abundances. In total, eight HStr stars can be employed for our investigation of neutron-capture nucleosynthesis in this substructure.

The [Eu/Fe] as a function of metallicity is displayed in the bottom left panel of Figure 4. Every analyzed member of HStr has [Eu/Fe] > +0.3, with a median value of +0.5 and median absolute deviation of ±0.1. This is, indeed, consistent with the

other dSph galaxies in the SAGA database within the same metallicity range. However, field metal-poor stars are known for having ⟨[Eu/Fe]⟩ ∼ +0.4 (Shetrone 1996; Fulbright 2000; Sneden et al. 2008), which is unsurprising given the understanding that the Galactic halo was formed from the accretion of many small dwarf galaxies. Therefore, the elevated Eu abundance alone is not necessarily indicative of the same progenitor, unlike the peculiar [α/Fe]–[Fe/H] tendency discussed in Section 3.2. The most metal-poor star in the sample, despite showing higher levels of Eu enrichment ([Eu/Fe] = +1.1), has [Eu/H] similar to other low-metallicity ([Fe/H] < −1.2) stars of HStr. Nevertheless, more observations

of very metal-poor ([Fe/H] < −2.0) stars from this substructure and, of course, detection of Eu will certainly help constrain the conditions that existed in the early chemical-enrichment site(s) of its parent system.

We can investigate the predominance between the *s*- and the *r*-processes in the neutron-capture nucleosynthesis through [Ba/Eu]. Stars with [Ba/Eu] > 0.0 were enriched mostly via the *s*-process, while the birth environments of those with [Ba/Eu] < 0.0 were polluted primarily by the *r*-process (Spite 1992; see Sneden et al. 2008 and Frebel 2018 for reviews). In the bottom right panel of Figure 4, we present the [Ba/Eu]–[Fe/H] plane. All stars of HStr with [Fe/H] < −1.2 occupy the subsolar region of this parameter space. Therefore, these are moderately RPE (+0.3 < [Eu/Fe] ⩽ +1.0) metal-poor stars, attributed to the so-called *r*-I regime (Beers & Christlieb 2005). The only exception is the lowest-metallicity one that belongs to the highly RPE category (*r*-II; [Eu/Fe] > +1.0).

Another important discovery is that stars of HStr follow a similar sequence in [Ba/Eu] as a function of [Fe/H] to that of Sculptor (also perceptible from Figure 4), increasing toward higher metallicities. The single star with [Ba/Eu] > 0.0 is the most metal-rich in the sample, but is also consistent with Sculptor for this [Fe/H]. Accounting for possible systematic effects could shift the [Ba/Eu] down by up to ∼0.4 dex by, for instance, considering nonlocal thermodynamic equilibrium in the abundance calculations (Mashonkina & Christlieb 2014). Despite that, the result that most stars from HStr experienced strong chemical enrichment via the *r*-process would not be altered. Furthermore, the [Ba/Eu] of HStr members would still be in good agreement with stars from Sculptor. This finding corroborates the hypothesis that this surviving satellite of the Milky Way experienced an evolution similar to the progenitor of the stream. If Sculptor is a textbook dSph galaxy (Hill et al. 2019), HStr might be the remnant of an ancient system of a similar kind. Hence, spectroscopic studies of its member stars provide a way to refine our understanding about dSph galaxies in general. Most importantly, it represents a marvelous opportunity to study the emergence of *r*-process elements in these environments, especially at the lowest metallicities, but with stars bright enough to have high-resolution spectra readily acquired from ground-based facilities. In the context of the recent observations of gravitational waves (Abbott et al. 2017a), alongside an electromagnetic counterpart (Abbott et al. 2017b), of a neutron star merger (GW170817), comparison to *r*-process nucleosynthesis frequencies and yields should help elucidate whether or not this source is responsible, and to what degree, for the production of heavy atomic nuclei.

Likewise, we can compare the [Ba/Fe] and [Eu/Fe] ratios in the stream with those from other prominent kinematic/dynamical halo substructures, also suggested to be of accreted origin. In the bottom row of Figure 4, we display the [Eu/Fe] and [Ba/Eu] for metal-poor stars from Gaia-Sausage/Encela-dus (Belokurov et al. 2018; Helmi et al. 2018) and Sequoia (Myeong et al. 2019) with neutron-capture abundances recently published by Aguado et al. (2021a). These targets cover a narrow metallicity range, within −2.2 < [Fe/H] ≲ −1.5, but comparable to the interval for most HStr stars with such elements available. Overall, these stars from both Gaia-Sausage/Enceladus and Sequoia are, apparently, more *r*-process rich (medians of +0.6 and −0.7 for [Eu/Fe] and [Ba/Eu], respectively) than those of HStr (+0.5 and −0.4) for similar [Fe/H] values. However, given the small numbers

considered, it is difficult to achieve meaningful conclusions at this time.

During the preparation of this manuscript, Gull et al. (2021) made available Eu abundances for stars claimed to be associated with HStr. However, their target-selection function was based on pre-Gaia data and they did not employ a dynamical selection approach, relying solely on kinematics. After reevaluating their stars, only 2 out of their 12 candidates would be classified as members according to our criteria, both of which were already being considered in our study since they were previously recognized by either Roederer et al. (2010; CD–36 1052) or Limberg et al. (2021a; HE 0324–0122). As a consequence, the authors were unable to identify an *α* knee for a similar metallicity range. Also, many of their stars clearly deviate in both [Eu/Fe] and [Ba/Eu], showing no cohesive sequence as a function of [Fe/H] and a large spread.

Other recent works have utilized orbital and/or phase-space criteria to select members of halo substructures and/or stellar streams for high-resolution spectroscopy (e.g., Monty et al. 2020). However, such efforts are still incipient. This work sheds light on the possibility of taking advantage of dynamical information to, for instance, accelerate the discovery of RPE stars (see the discussion by Limberg et al. 2021b). Moreover, since these objects likely share a common origin, this approach should be more useful than randomly drawing from extensive lists of cool low-metallicity stars (Limberg et al. 2021b).

## 4. Summary

In this Letter, we employed astrometric and spectroscopic data from Gaia EDR3 and GALAH+ DR3, respectively, to identify eight new members of HStr, which allows us to cover a considerably wider (by ∼0.5 dex) metallicity interval (−2.5 ≲ [Fe/H] < −1.0) than previously reported by Aguado et al. (2021b). We also reevaluated candidates from the literature to consolidate a sample of 22 stars of this substructure. Thanks to the now-extended metallicity range, our study clearly shows a declining trend in [*α*/Fe] (Mg and Ca) with increasing [Fe/H]. Considering exclusively the newly found members from GALAH, this pattern is still noticeable. Consequently, our qualitative conclusions are valid even in the presence of small biases between abundances extracted from different sources. We were also able to confirm that stars of HStr constitute an *α*-element pattern similar to the Sculptor dSph galaxy up to [Fe/H] ∼ −1.0. This apparent dSph origin is in good agreement with *N*-body simulations (Koppelman et al. 2019) of this merging event.

We confirm that, at low metallicities ([Fe/H] ≲ −1.2), the progenitor system of HStr experienced enrichment in neutron-capture elements predominantly via the *r*-process, as first conjectured by Roederer et al. (2010). All analyzed stars in this metallicity regime are RPE ones, with median values for [Eu/Fe] and [Ba/Eu] of +0.5 and −0.4, respectively. The behavior of HStr in [Ba/Eu]–[Fe/H] is also coherent with stars from Sculptor. In particular, the extended metallicity range suggests an increase in [Ba/Eu] for higher [Fe/H], reinforcing the hypothesis that the stream originated from the disruption of a dwarf galaxy of a similar kind. Finally, stars from Gaia-Sausage/Enceladus and Sequoia are, apparently, more *r*-process rich than HStr ones. In the upcoming years, stars from these accreted halo substructures will serve as important laboratories to understand the early nucleosynthesis of heavy

elements in their long-vanished dwarf-galaxy progenitor systems.

## Appendix
## Final List of Members

Table 1 contains relevant information about our compilation of stars of HStr from both GALAH and the literature, including uncertainties. The universal identifier for these objects is their Gaia EDR3 IDs. In the second column, we provide the classification of the stars either as confident (1) or likely (2) members (Section 3.1). Positions ($\alpha$, $\delta$), proper motions ($\mu_\alpha \cos \delta$, $\mu_\delta$), and parallaxes ($\varpi$; recalibrated following Lindegren et al. 2021a) are included as well. The adopted RV values are also listed. Heliocentric distances ($d_{\rm SH}$) estimated with StarHorse are in the ninth column. Lower and upper limits for these quantities represent the 16th and 84th percentiles of their distributions. The stellar atmospheric parameters and elemental abundances determined from the analyses of the high-resolution spectra (Section 2.1) of the studied stars are provided by the end of the table.

**Table 1**
Consolidated List of Helmi Stream Members

| Star Name (Gaia EDR3) | Class | α (deg) | δ (deg) | $\mu_\alpha \cos\delta$ (mas yr⁻¹) | $\mu_\delta$ (mas yr⁻¹) | $\varpi$ (mas) | RV (km s⁻¹) | $d_{SH}$ (kpc) | $T_{eff}$ (K) | log g (cgs) | [Fe/H] | [Mg/Fe] | [Ca/Fe] | [Ba/Fe] | [Eu/Fe] |
|---|---|---|---|---|---|---|---|---|---|---|---|---|---|---|---|
| 2336548524982631808 | 2 | 0.5695 | −24.8971 | −3.635 ± 0.013 | −8.153 ± 0.012 | 0.178 ± 0.024 | 78.8 ± 2.0 | $5.84^{+0.74}_{-0.54}$ | 5020 ± 100 | 1.73 ± 0.30 | −1.81 ± 0.19 | ... | ... | +0.10 ± 0.10 | +0.52 ± 0.20 |
| 2543922018619120000 | 1 | 6.5826 | 0.6263 | 7.200 ± 0.045 | −22.060 ± 0.035 | 0.574 ± 0.059 | 168.0 ± 3.0 | $1.73^{+0.13}_{-0.17}$ | 6305 ± 102 | 4.04 ± 0.52 | −2.02 ± 0.10 | +0.38 ± 0.05 | +0.36 ± 0.12 | −0.40 ± 0.10 | ... |
| 2781151719714308352 | 1[a] | 12.4166 | 15.5549 | 7.534 ± 0.055 | −29.597 ± 0.034 | 0.644 ± 0.053 | 114.0 ± 3.0 | $1.55^{+0.11}_{-0.13}$ | 6315 ± 102 | 4.06 ± 0.52 | −1.94 ± 0.11 | +0.38 ± 0.07 | +0.36 ± 0.09 | −0.39 ± 0.11 | ... |
| 2537418854016682368 | 1 | 15.0695 | 1.2378 | 1.247 ± 0.038 | −20.811 ± 0.031 | 0.469 ± 0.032 | 187.3 ± 1.0 | $2.16^{+0.17}_{-0.21}$ | 5299 ± 189 | 3.52 ± 0.26 | −1.14 ± 0.22 | +0.06 ± 0.24 | +0.02 ± 0.14 | −0.34 ± 0.20 | ... |
| 2518385517465704960 | 1 | 31.7239 | 4.5957 | −6.045 ± 0.043 | −37.618 ± 0.032 | 0.828 ± 0.053 | 181.8 ± 5.0 | $1.20^{+0.06}_{-0.06}$ | 6143 ± 105 | 4.63 ± 0.51 | −1.99 ± 0.11 | +0.31 ± 0.08 | +0.16 ± 0.09 | −0.29 ± 0.10 | ... |
| 4698632984741726976 | 2[a] | 40.8047 | −65.1743 | −0.895 ± 0.015 | 3.278 ± 0.013 | 0.157 ± 0.013 | 255.2 ± 0.7 | $6.18^{+0.61}_{-0.74}$ | 4898 ± 128 | 2.09 ± 0.24 | −1.14 ± 0.13 | −0.09 ± 0.14 | +0.02 ± 0.11 | +0.40 ± 0.14 | ... |
| 2497639347957300096 | 2 | 41.3709 | −1.0151 | 3.173 ± 0.019 | −9.668 ± 0.015 | 0.287 ± 0.027 | 205.6 ± 0.1 | $3.84^{+0.12}_{-0.12}$ | 4168 ± 15 | 0.77 ± 0.10 | −1.69 ± 0.10 | +0.14 ± 0.02 | −0.03 ± 0.05 | ... | ... |
| 4690890363997251200 | 1[a] | 41.4447 | −65.5653 | −2.994 ± 0.014 | 1.705 ± 0.012 | 0.150 ± 0.013 | 143.0 ± 0.5 | $6.76^{+0.54}_{-0.74}$ | 4463 ± 95 | 1.19 ± 0.25 | −2.04 ± 0.08 | +0.13 ± 0.06 | +0.24 ± 0.07 | +0.51 ± 0.08 | +0.67 ± 0.09 |
| 5049085217270417152 | 1 | 41.9060 | −36.1075 | 3.187 ± 0.010 | 12.591 ± 0.014 | 1.380 ± 0.023 | 304.7 ± 0.8 | $0.73^{+0.01}_{-0.01}$ | 6070 ± 200 | 2.30 ± 0.30 | −1.65 ± 0.10 | +0.36 ± 0.10 | +0.33 ± 0.10 | +0.13 ± 0.15 | +0.48 ± 0.10 |
| 3267948604442696448 | 1 | 51.7594 | 1.5422 | −19.554 ± 0.015 | −41.520 ± 0.014 | 0.968 ± 0.025 | 186.2 ± 2.0 | $1.04^{+0.02}_{-0.03}$ | 5170 ± 100 | 2.50 ± 0.30 | −2.39 ± 0.13 | +0.29 ± 0.15 | +0.28 ± 0.15 | +0.50 ± 0.20 | +1.07 ± 0.20 |
| 4668621380510613248 | 2[a] | 64.7304 | −67.3146 | −1.803 ± 0.017 | −0.399 ± 0.015 | 0.136 ± 0.016 | 148.1 ± 0.4 | $6.19^{+0.54}_{-0.63}$ | 4738 ± 91 | 1.79 ± 0.26 | −1.15 ± 0.07 | −0.11 ± 0.05 | +0.03 ± 0.06 | +0.58 ± 0.06 | +0.33 ± 0.08 |
| 2959451922593403904 | 2[a] | 77.0546 | −25.5669 | −9.151 ± 0.012 | −13.330 ± 0.014 | 0.315 ± 0.017 | 100.4 ± 0.6 | $3.36^{+0.25}_{-0.29}$ | 4859 ± 111 | 2.00 ± 0.23 | −2.27 ± 0.12 | +0.23 ± 0.10 | +0.30 ± 0.07 | −0.07 ± 0.08 | ... |
| 680735037764135808 | 1 | 122.1393 | 24.3130 | −49.704 ± 0.026 | −37.350 ± 0.019 | 1.130 ± 0.037 | −88.1 ± 5.0 | $0.88^{+0.03}_{-0.03}$ | 6070 ± 102 | 4.50 ± 0.51 | −2.38 ± 0.10 | +0.38 ± 0.07 | +0.34 ± 0.14 | +0.50 ± 0.13 | ... |
| 814087862430876160 | 1 | 142.4193 | 41.0978 | −39.395 ± 0.027 | −20.315 ± 0.021 | 1.186 ± 0.041 | −222.0 ± 3.0 | $0.88^{+0.02}_{-0.03}$ | 5973 ± 105 | 4.64 ± 0.51 | −2.19 ± 0.11 | +0.34 ± 0.06 | +0.26 ± 0.12 | +0.40 ± 0.14 | ... |
| 5399644708578669696 | 1[a] | 170.7452 | −34.1081 | −11.629 ± 0.014 | −5.05 ± 0.011 | 0.183 ± 0.016 | 70.8 ± 0.4 | $5.23^{+0.44}_{-0.45}$ | 4523 ± 87 | 1.45 ± 0.31 | −1.24 ± 0.07 | +0.18 ± 0.05 | +0.07 ± 0.06 | +0.11 ± 0.07 | +0.32 ± 0.08 |
| 840612307043955552 | 1 | 177.6522 | 54.1241 | −3.861 ± 0.011 | −1.818 ± 0.012 | 0.306 ± 0.022 | −277.7 ± 0.1 | $2.85^{+0.16}_{-0.27}$ | 4907 ± 25 | 2.16 ± 0.10 | −1.14 ± 0.10 | −0.08 ± 0.02 | +0.16 ± 0.03 | ... | ... |
| 6153268944831195648 | 2[a] | 190.2765 | −38.6669 | −9.576 ± 0.015 | −11.931 ± 0.012 | 0.256 ± 0.018 | −43.7 ± 0.6 | $4.13^{+0.36}_{-0.43}$ | 4897 ± 131 | 2.26 ± 0.10 | −1.38 ± 0.12 | +0.14 ± 0.11 | +0.15 ± 0.10 | +0.04 ± 0.12 | ... |
| 3630429997250686592 | 2[a] | 202.5277 | −7.6950 | −6.231 ± 0.025 | −6.512 ± 0.014 | 0.194 ± 0.023 | −228.9 ± 0.9 | $5.43^{+0.76}_{-0.59}$ | 4962 ± 193 | 2.43 ± 0.33 | −1.26 ± 0.20 | +0.29 ± 0.23 | +0.28 ± 0.14 | +0.05 ± 0.20 | ... |
| 3742101345970116224 | 1 | 205.8611 | 15.5752 | −49.997 ± 0.017 | −14.872 ± 0.011 | 1.898 ± 0.029 | −285.9 ± 0.8 | $0.54^{+0.01}_{-0.00}$ | 5290 ± 200 | 1.10 ± 0.30 | −2.15 ± 0.10 | +0.34 ± 0.10 | +0.33 ± 0.10 | −0.02 ± 0.24 | +0.34 ± 0.10 |
| 1275876252107941888 | 1 | 226.7244 | 30.0102 | 13.941 ± 0.009 | −7.761 ± 0.013 | 0.683 ± 0.027 | −280.3 ± 0.8 | $1.47^{+0.06}_{-0.06}$ | 4330 ± 200 | 0.60 ± 0.30 | −1.45 ± 0.10 | +0.31 ± 0.16 | +0.29 ± 0.10 | +0.06 ± 0.25 | +0.65 ± 0.15 |
| 17702675557939840 | 1 | 322.8380 | 13.1278 | 4.082 ± 0.012 | −16.745 ± 0.010 | 0.258 ± 0.022 | 71.4 ± 0.1 | $4.06^{+0.18}_{-0.34}$ | 4975 ± 16 | 1.82 ± 0.10 | −1.85 ± 0.10 | +0.18 ± 0.03 | +0.01 ± 0.07 | ... | ... |
| 6536758912468029184 | 1 | 351.2973 | −39.9912 | 4.400 ± 0.023 | −7.736 ± 0.028 | 0.561 ± 0.022 | 286.8 ± 0.8 | $1.80^{+0.10}_{-0.12}$ | 6650 ± 200 | 3.70 ± 0.30 | −2.55 ± 0.10 | +0.32 ± 0.10 | +0.41 ± 0.12 | −0.31 ± 0.30 | ... |

**Notes.**
[a] Newly recognized members in this work.

## ORCID iDs

Guilherme Limberg ⦿ https://orcid.org/0000-0002-9269-8287
Rafael M. Santucci ⦿ https://orcid.org/0000-0002-7529-1442
Silvia Rossi ⦿ https://orcid.org/0000-0001-7479-5756
Cristina Chiappini ⦿ https://orcid.org/0000-0003-1269-7282
Stefano O. Souza ⦿ https://orcid.org/0000-0001-8052-969X
Hélio D. Perottoni ⦿ https://orcid.org/0000-0002-0537-4146
Angeles Pérez-Villegas ⦿ https://orcid.org/0000-0002-5974-3998
Fabrícia O. Barbosa ⦿ https://orcid.org/0000-0002-8262-2246

## References

Abbott, B. P., Abbott, R., Abbott, T. D., et al. 2017a, PhRvL, 119, 161101
Abbott, B. P., Abbott, R., Abbott, T. D., et al. 2017b, ApJL, 848, L12
Aguado, D. S., Belokurov, V., Myeong, G. C., et al. 2021a, ApJL, 908, L8
Aguado, D. S., Myeong, G. C., Belokurov, V., et al. 2021b, MNRAS, 500, 889
Beers, T. C., & Christlieb, N. 2005, ARA&A, 43, 531
Belokurov, V., Erkal, D., Evans, N. W., Koposov, S. E., & Deason, A. J. 2018, MNRAS, 478, 611
Buder, S., Sharma, S., Kos, J., et al. 2021, MNRAS, in press (doi:10.1093/mnras/stab1242)
Cui, X.-Q., Zhao, Y.-H., Chu, Y.-Q., et al. 2012, RAA, 12, 1197
Ezzeddine, R., Rasmussen, K., Frebel, A., et al. 2020, ApJ, 898, 150
Frebel, A. 2018, ARNPS, 68, 237
Fulbright, J. P. 2000, AJ, 120, 1841
Gaia Collaboration, Brown, A. G. A., Vallenari, A., et al. 2021, A&A, 649, A1
Gudin, D., Shank, D., Beers, T. C., et al. 2021, ApJ, 908, 79
Gull, M., Frebel, A., Hinojosa, K., et al. 2021, ApJ, 912, 52
Hansen, T. T., Holmbeck, E. M., Beers, T. C., et al. 2018, ApJ, 858, 92
Helmi, A. 2008, A&ARv, 15, 145
Helmi, A. 2020, ARA&A, 58, 205
Helmi, A., Babusiaux, C., Koppelman, H. H., et al. 2018, Natur, 563, 85
Helmi, A., White, S. D. M., de Zeeuw, P. T., & Zhao, H. 1999, Natur, 402, 53
Hill, V., Skúladóttir, Á., Tolstoy, E., et al. 2019, A&A, 626, A15
Ji, A. P., Frebel, A., Simon, J. D., & Chiti, A. 2016, ApJ, 830, 93
Koppelman, H. H., Helmi, A., Massari, D., Roelenga, S., & Bastian, U. 2019, A&A, 625, A5
Lemasle, B., de Boer, T. J. L., Hill, V., et al. 2014, A&A, 572, A88
Letarte, B., Hill, V., Tolstoy, E., et al. 2010, A&A, 523, A17
Limberg, G., Rossi, S., Beers, T. C., et al. 2021a, ApJ, 907, 10
Limberg, G., Santucci, R. M., Rossi, S., et al. 2021b, ApJ, 913, 11
Lindegren, L., Bastian, U., Biermann, M., et al. 2021a, A&A, 649, A4
Lindegren, L., Klioner, S. A., Hernández, J., et al. 2021b, A&A, 649, A2
Majewski, S. R., Schiavon, R. P., Frinchaboy, P. M., et al. 2017, AJ, 154, 94
Mashonkina, L., & Christlieb, N. 2014, A&A, 565, A123
Matteucci, F., & Brocato, E. 1990, ApJ, 365, 539
Matteucci, F., & Greggio, L. 1986, A&A, 154, 279
McMillan, P. J. 2017, MNRAS, 465, 76
Monty, S., Venn, K. A., Lane, J. M. M., Lokhorst, D., & Yong, D. 2020, MNRAS, 497, 1236
Myeong, G. C., Evans, N. W., Belokurov, V., Amorisco, N. C., & Koposov, S. E. 2018, MNRAS, 475, 1537
Myeong, G. C., Vasiliev, E., Iorio, G., Evans, N. W., & Belokurov, V. 2019, MNRAS, 488, 1235
Queiroz, A. B. A., Anders, F., Chiappini, C., et al. 2020, A&A, 638, A76
Queiroz, A. B. A., Anders, F., Santiago, B. X., et al. 2018, MNRAS, 476, 2556
Roederer, I. U., Sneden, C., Thompson, I. B., Preston, G. W., & Shectman, S. A. 2010, ApJ, 711, 573
Rybizki, J., Green, G., Rix, H.-W., et al. 2021, arXiv:2101.11641
Schönrich, R., Binney, J., & Dehnen, W. 2010, MNRAS, 403, 1829
Shetrone, M., Venn, K. A., Tolstoy, E., et al. 2003, AJ, 125, 684
Shetrone, M. D. 1996, AJ, 112, 1517
Skrutskie, M. F., Cutri, R. M., Stiening, R., et al. 2006, AJ, 131, 1163
Sneden, C., Cowan, J. J., & Gallino, R. 2008, ARA&A, 46, 241
Spite, M. 1992, in Proc. IAU Symp 149, The Stellar Populations of Galaxies, ed. B. Barbuy & A. Renzini (Dordrecht: Kluwer), 123
Spite, M., & Spite, F. 1978, A&A, 67, 23
Suda, T., Hidaka, J., Aoki, W., et al. 2017, PASJ, 69, 76
Suda, T., Katsuta, Y., Yamada, S., et al. 2008, PASJ, 60, 1159
Tolstoy, E., Hill, V., & Tosi, M. 2009, ARA&A, 47, 371
Vasiliev, E. 2019, MNRAS, 482, 1525
Wright, E. L., Eisenhardt, P. R. M., Mainzer, A. K., et al. 2010, AJ, 140, 1868
Yanny, B., Rockosi, C., Newberg, H. J., et al. 2009, AJ, 137, 4377
York, D. G., Adelman, J., Anderson, John E., J., et al. 2000, AJ, 120, 1579
Yuan, Z., Myeong, G. C., Beers, T. C., et al. 2020, ApJ, 891, 39